J Membrane Biol (2011) 244:67–80
DOI 10.1007/s00232-011-9399-x

Bacterial Expression, Purification and Characterization of a Rice Voltage-Dependent, Anion-Selective Channel Isoform, OsVDAC4

Ashwini Godbole · Rohan Mitra · Ashvini K. Dubey · Palakolanu S. Reddy · M. K. Mathew

Received: 28 May 2011 / Accepted: 15 October 2011 / Published online: 6 November 2011
© Springer Science+Business Media, LLC 2011

Abstract The voltage-dependent anion-selective channel (VDAC) is the most abundant protein in the mitochondrial outer membrane and forms the major conduit for metabolite transport across this membrane. VDACs from different sources show varied primary sequence but conserved functional properties. Here, we report on the characterization of a rice channel, OsVDAC4, which complements a VDAC1 deficiency in yeast. We present a consensus secondary structure prediction of an N-terminal α-helix and 19 β-strands. Bacterially expressed OsVDAC4 was purified from inclusion bodies into detergent-containing solution, where it is largely helical. Detergent-solubilized OsVDAC4 inserts spontaneously into artificial membranes of two topologies—spherical liposomes and planar bilayers. Insertion into liposomes results in an increase in β-structure. Transport of polyethylene glycols was used to estimate a pore diameter of ~2.6 nm in liposomes. Channels formed in planar bilayers exhibit large conductance (4.6 ± 0.3 nS in 1 M KCl), strong voltage dependence and weak anion selectivity. The open state of the channel is shown to be permeable to ATP. These data are consistent with a large β-barrel pore formed by OsVDAC4 on inserting into membranes. This study forms a platform to carry out studies of the interaction of OsVDAC4 with putative modulators.

Keywords OsVDAC4 · Mitochondria · β-barrel · Liposome swelling · Planar bilayer membrane · Anion-selective · ATP

R. Mitra and A. K. Dubey contributed equally to this research.

A. Godbole · R. Mitra · A. K. Dubey · P. S. Reddy · M. K. Mathew (✉)
National Centre for Biological Sciences, TIFR, UAS-GKVK Campus, Bangalore 560065, India
e-mail: mathew@ncbs.res.in

Present Address:
A. Godbole
Centre for Pharmacognosy, Pharmaceutics and Pharmacology, Institute of Ayurveda and Integrative Medicine, No. 74/2, Jarakbande Kaval, Post: Attur, Via Yelahanka, Bangalore 560064, India

Present Address:
R. Mitra
Department of Human Genetics, National Institute of Mental Health and Neurosciences (NIMHANS), Bangalore 560029, India

Present Address:
P. S. Reddy
Department of Biotechnology, Molecular Therapeutic Laboratory, School of Life Science, University of Hyderabad, Gachhibowli, Hyderabad 500046, India

Introduction

The voltage-dependent, anion-selective channel (VDAC) is a major protein of the outer mitochondrial membrane (OMM) and mediates transport of hydrophilic metabolites in all eukaryotic organisms (Colombini 2004; Shoshan-Barmatz and Gincel 2003; Vander Heiden et al. 2000). In addition, its role in many physiological processes, including calcium homeostasis (Cesura et al. 2003; Gincel et al. 2001; Rapizzi et al. 2002; Shoshan-Barmatz and Israelson 2005) and programmed cell death (Shimizu et al. 2001; Shoshan-Barmatz and Gincel 2003; Vander Heiden et al. 2001), has been elucidated over the past three decades. VDACs from different sources vary greatly in their primary

amino acid sequence, but all are predicted to form β-barrel pores in the membrane (Young et al. 2007).

All VDACs characterized so far exhibit eponymous voltage-dependent conductance in artificial membrane systems. The pore is maximally conductive under zero field conditions and undergoes transitions to lower conductance states under high imposed transmembrane electric fields of either polarity. The low field open state is weakly anion-selective and can conduct ATP and ADP, whereas the principal low-conductance substate is cation-permeable and does not conduct nucleotides (Rostovtseva and Colombini 1996; Rostovtseva and Bezrukov 1998).

In animals, a case for a VDAC role in many pathological conditions, like neurodegenerative disease and cancer, has been built up over more than a decade (Keinan et al. 2010; Madesh and Hajnoczky 2001; Shoshan-Barmatz et al. 2008; Veenman et al. 2008). Changes in VDAC function in different pathophysiological conditions have been characterized and the factors modulating these changes identified in many instances (Shoshan-Barmatz and Gincel 2003; Vander Heiden et al. 2001). VDAC is also present in plant cells, with transcripts found in all organs tested under normal physiological conditions. However, unlike in animal cells, its subcellular localization can be diverse. Indeed, in *Lotus japonicus* root nodule cells, VDAC or VDAC-like proteins are found not only in mitochondrial membranes but also in plastids and, in some cell types, even on membrane vesicles (Wandrey et al. 2004).

Transcript levels of VDAC change significantly across developmental stages as in the course of floral development (Elkeles et al. 1997; Kushalappa et al. 2000) as well as under a range of physiological conditions such as cell death (Lee et al. 2009). Changes in the expression level of VDAC have also been documented in response to biotic stress, as in the hypersensitive response to pathogen attack (Lee et al. 2009). Additionally, in *Pennisitum glaucum*, VDAC is overexpressed under abiotic stresses imposed by salinity and cold (Desai et al. 2006), while expression of rice VDAC increases during recovery from osmotic stress (Al Bitar et al. 2003). Interestingly, overexpression of *P. glaucum* VDAC in rice plants confers tolerance to salinity stress (Desai et al. 2006). Further, tRNA transport into mitochondria is mediated through VDAC in *Solanum tuberosum* (Salinas et al. 2006).

In animal cells, VDAC has been shown to play a critical role in Bcl-2-family protein–mediated mitochondrial cell death pathways (Shimizu et al. 2001; Vander Heiden et al. 2001). A role for VDAC in plant cell death is becoming clear, especially during the hypersensitive response to pathogen attack (Lee et al. 2009). Although plants do not have Bcl-2-family proteins, heterologous expression of Bax leads to cell death in *Nicotiana benthamina* leaves (Lacomme and Santa Cruz 1999). This death program requires the presence of VDAC (Tateda et al. 2009). Further, we have shown that overexpression of a rice VDAC isoform, OsVDAC4, can induce cell death in a mammalian cell line. This death program can be modulated by mammalian Bcl-2 proteins (Godbole et al. 2003). A conserved role for VDAC in cell death is thus indicated.

The wide variety of cellular processes in plants that are influenced by VDAC is not accompanied by a corresponding understanding of its properties or the factors modulating its function. Extensive in vitro biophysical and biochemical studies along with in vivo cell biological experiments would be required to get a better understanding of VDAC function. VDAC isoforms from a few plants, like wheat (Elkeles et al. 1997), potato (Heins et al. 1994), corn (Geiger et al. 1999), lentil (Wandrey et al. 2004) and mung bean (Zalman et al. 1980), have been characterized using biophysical techniques on purified and reconstituted protein. In most cases this is restricted to electrophysiological studies on protein incorporated in bilayer lipid membranes (BLMs). All plant VDACs characterized so far show properties similar to those from fungal and animal sources. Interestingly, potato VDAC is sensitive to soluble mitochondrial factors from fungal and mammalian cells in addition to its own proteins (Liu and Colombini 1991).

Four isoforms of VDAC have been identified in rice (Al Bitar et al. 2003; Cooper et al. 2003). Molecular characterization and expression profile studies of OsVDAC1–3 have been done, but none has been characterized biophysically. In the present study, we report on the characterization of a rice VDAC isoform, OsVDAC4. This VDAC isoform was overexpressed during inflorescence development (Kushalappa et al. 2000). It was also overexpressed during stress response and seed development (Cooper et al. 2003). In an earlier study, we showed that OsVDAC4 localizes to mitochondria and functions in an apoptotic context when expressed in a lymphocyte cell line (Godbole et al. 2003). Here, we report on bacterial expression and purification of OsVDAC4 and characterize it functionally by reconstitution into two complementary artificial membrane systems, liposomes and planar bilayers. The former permits the monitoring of solute transport, while the latter provides information on electrical conductivity. This study provides a platform for probing interactions of VDAC with the proteins and small molecules implicated in modulating its function within the cell.

Materials and Methods

Sequence Analysis and Secondary Structure Prediction

OsVDAC4 cDNA, isolated from a rice inflorescence library, was a gift from Prof. Usha Vijayraghavan (Indian

Institute of Science, Bangalore, India). The cDNA was sequenced using the dideoxy method in an automated DNA sequencer (Applied Biosciences, Hitachi, Foster City, CA). A BLAST search using the longest predicted open reading frame in the sequence came up with multiple hits.

Multiple sequence alignment of the VDAC sequences found by the BLAST search was done using ClustalW2 (http://www.ebi.ac.uk/Tools/clustalw2/). A phylogenetic tree was constructed based on the amino acid identity between different VDACs using ClustalW2 and was viewed by using JavaView (http://www.ebi.ac.uk/Tools/es/cgi-bin/jobresults.cgi/clustalw2/clustalw2-20100511-0314452494.aln).

Hydropathy analysis of the OsVDAC4 protein sequence was done using the Kyte-Doolittle algorithm (http://expasy.org/cgi-bin/protscale.pl?1). The OsVDAC4 sequence was submitted to five different servers for secondary structure prediction: PSIPRED (http://bioinf.cs.ucl.ac.uk/psipred), YASPIN (http://www.ibi.vu.nl/programs/yaspinwww/), APSSP2 (http://www.imtech.res.in/raghava/apssp2/), PredictProtein (http://www.predictprotein.org/) and PORTER (http://distill.ucd.ie/porter/). Residues predicted to be present in a secondary structure element by three or more of the algorithms were deemed to be part of that structural element to make a consensus prediction.

Expression and Purification of OsVDAC4

The open reading frame of the cDNA without the stop codon was cloned in-frame with the pelB leader sequence, upstream of a histidine tag in the bacterial expression vector pET-20b+ (Novagen, Milwaukee, WI) between *Nco*I and *Xho*I sites. The resultant OsVDAC4-pET-20b+ construct was then transformed into *Escherichia coli* host strain BL21 (DE3)-pLysS and grown in the presence of 100 μg/ml ampicillin and 25 μg/ml chloramphenicol.

For expression of protein, bacterial growth and induction were carried out at 37°C. Overnight cultures were diluted 100-fold (1 l final volume) into fresh LB medium (containing 100 μg/ml ampicillin and 25 μg/ml chloramphenicol) and grown to a final A_{600} of 0.4–0.5. IPTG (1 mM) was added to induce expression of the protein, and cultures were further incubated for 3 h. Cells were then placed on ice for 5–10 min and centrifuged at 6,000 x *g* for 30 min at 4°C. Pellets were resuspended in 40 ml of ice-cold buffer A [20 mM Tris-HCl (pH 7.0), 2 mM $MgCl_2$, 0.1 mM EDTA, 1 mM DTT and 1 mM PMSF]. Cells were sonicated at 40% amplitude for 10 min with a 5-s on/off cycle and a high gain probe of the sonicator (Vibra-Cell; Sonics, Newtown, CT). The lysate was centrifuged at 6,000×*g* for 30 min to remove unlysed cells. The supernatant was then spun at 16,000×*g* for 30 min to obtain the inclusion body fraction. Inclusion bodies were washed twice with 2 mM $CaCl_2$ and then solubilized in 75 ml of solubilization buffer [50 mM Tris–HCl (pH 8.0), 100 mM NaCl, 6 M GnHCl] for 1 h. Solubilized inclusion bodies (75 ml) containing His-tagged OsVDAC4 proteins were diluted with 25 ml of solubilization buffer without GnHCl and added to 20 ml (bed volume) of equilibrated Ni-NTA resin (Qiagen, Palo Alto, CA). After 1 h of binding, the matrix was packed in a column (16 mm diameter) and washed with three volumes of column buffer [4.5 M GnHCl, 100 mM NaCl, 20 mM Tris–HCl (pH 8.0)] containing 10 mM imidazole. His-tagged OsVDAC4 was eluted with two volumes of column buffer containing 50 mM imidazole. Protein concentration was measured by Bradford assay (Bangalore Genei, Bangalore, India). Protein fractions were concentrated to 6–8 mg/ml by centrifugation in Centricon 30 tubes (Millipore, Bedford, MA). LDAO was added to a final concentration of 2% and GnHCl removed by dialysis against loading buffer. Proteins were stored at –80°C at a concentration of 1–5 mg/ml.

Mass Spectrometry

Ni-NTA-purified OsVDAC4 was run on SDS-PAGE and stained with Coomassie brilliant blue. The band corresponding to 29 kDa molecular weight was excised and diced into small pieces. Gel pieces were washed multiple times with ~500 μl of wash solution (50 mM NH_4HCO_3 in 50% acetonitrile) to remove Coomassie blue and dehydrated with 100% acetonitrile. Destained gel was dried completely at room temperature for 10–20 min in a centrifugal evaporator. The gel was rehydrated in 150 μl reduction solution (10 mM DTT, 100 mM ammonium bicarbonate) for 30 min at 56°C. Gel pieces were then incubated with 100 μl of alkylation solution (50 mM iodoacetamide, 100 mM ammonium bicarbonate) for 30 min and washed with wash solution, followed by dehydration with 100% acetonitrile. Gel pieces were dried completely and incubated with freshly diluted protease digestion solution (20 μg trypsin in 1 ml of 50 mM NH_4HCO_3) at 37°C for 16–20 h. To extract the peptides, 25–50 μl of extraction solution (60% acetonitrile, 1% TFA) was added to gel pieces, which were then vortexed, sonicated and centrifuged. The supernatant was dried at room temperature to near dryness then resuspended in resuspension solution (50% acetonitrile, 1% TFA) and used for mass spectrometric analysis on an Ultraflex TOF/TOF spectrometer (Bruker Daltonics, Billerica, MA), equipped with a 50 Hz pulsed nitrogen laser (λ337 nm). Two peptides showing predicted mass were selected for sequencing by tandem mass spectrometry, MALDI-MS/MS.

Circular Dichroism Analysis

Far-UV circular dichroism spectra of OsVDAC4 incorporated into detergent micelles and liposomes were recorded on a Jasco 720 CD spectropolarimeter (Jasco, Easton, MD) at 20°C. OsVDAC4-containing liposomes were prepared as described below (see "Preparation of Unilamellar Liposomes and Protein Incorporation" section), except that dextran was not added in the buffer. Liposomes were centrifuged at 100,000×*g* for 1 h. The supernatant was removed, and liposomes were resuspended in an appropriate volume of buffer to obtain a protein concentration of approximately 1 μg/ml. OsVDAC4 (approximately 1 μg/ml) in LDAO micelles or in liposomes was taken in a 0.2-cm cuvette. Twenty scans were averaged for each spectrum, with a response time of 2 s, a bandwidth of 1.0 nm and a scan speed of 100 nm/min from 195 to 250 nm.

Construction of Yeast Expression Plasmids, Transformation and Characterization

The yeast strain M22.2, where the VDAC1 gene is deleted; the corresponding wild-type strain (M3); and the recombinant plasmid carrying wild-type yeast porin gene were kind gifts from Dr. E. Blachly-Dyson (Vollum Institute, Portland, OR). The recombinant plasmid that carries the wild-type yeast porin (VDAC1) gene was digested with *Nco*I and *Nsi*I to remove the coding region of yeast porin and replaced with OsVDAC4 cDNA which was digested with *Nco*1 and *Pst*1. Subsequently, the OsVDAC4 cDNA with yeast porin promoter and terminator was excised with *Bam*HI–*Hin*dIII and cloned into *Bam*HI–*Hin*dIII sites of pSEYC58, a yeast centromeric plasmid. These recombinant pSEYC58 plasmids expressing OsVDAC4 under the yeast porin promoter were introduced into M22.2 by the lithium acetate–mediated transformation protocol.

To confirm the expression of OsVDAC4 in M22.2, we performed RT-PCR using a standard RT-PCR protocol (http://openwetware.org/images/3/30/RNAextrc.pdf) of M3, M22.2 and M22.2-transformed OsVDAC4 with OsVDAC4-specific primer (forward 5′-GACCAGAAGCT GACCGTCTC-3′, reverse 5′-GCTTCGGGGTCAACCTT GTA-3′).

Preparation of Unilamellar Liposomes and Protein Incorporation

Unilamellar liposomes were made with soybean L-α lecithin phosphatidylcholine (Calbiochem, La Jolla, CA). Soy lecithin solution in chloroform (20 mg/ml) in a round-bottomed flask was dried under a jet of dry argon while being rotated so as to form a thin film. Lipid was kept overnight in a desiccator to ensure complete drying. The film of lipid was then dispersed in buffer [1 M KCl, 5 mM $MgCl_2$ and 5 mM HEPES (pH 7.4)] containing 3 mM 10,000 D dextran (Molecular Probes, Eugene, OR). Detergent-solubilized OsVDAC4 was added to the lipid mix at a 1:25 protein to lipid (w/w) ratio. In case of plain liposomes, an equal volume of buffer-containing detergent was added. The protein–lipid mixture was passed (23 passes) through a 0.2 μm polycarbonate filter in a liposome maker (Avanti Polar Lipids, Alabaster, AL) to obtain unilamellar liposomes. The lipid suspension, which was milky to begin with, turned opalescent after passing through the liposome maker. To obtain larger liposomes, the mixture was taken through three cycles of freezing in liquid nitrogen and thawing at 37°C. Liposomes were subsequently used for the liposome swelling assay.

Liposome Swelling Assay

The pore-forming activity of OsVDAC4 and the relative permeability of different polyethylene glycols (PEGs) through the channel were assessed by the liposome swelling assay (Nikaido and Rosenberg 1981; Tejuca et al. 2001). The dextran-incorporated liposomes were diluted into iso-osmotic buffer containing different PEGs. PEGs (HiMedia, Mumbai, India) used in this study were PEG400 (0.56 nm), PEG600 (0.59 nm), PEG1000 (0.776 nm), PEG3000 (1.05 nm) and PEG4000 (1.1 nm) (number in parentheses is the hydrated radius of the PEG). Absorbance at 520 nm was recorded at 2 s intervals for 10 min using a Cary 1 UV–Visible spectrophotometer (Varian, Sydney, Australia). The liposome mixture was stirred constantly to avoid settling and aggregation.

Estimation of Effective Diameter of the Pore Formed by OsVDAC4 in Liposomes

The effective pore diameter of the channel was estimated using Renkin formalism, which provides an estimate of the total restriction to diffusion due to the combined effects of steric hindrance at the entrance to the pores and frictional resistance within the pores. This is given by

$$A/A_o = [1 - (a/r)]^2\left[1 - 2.104(a/r) + 2.09(a/r)^3 - 0.95(a/r)^5\right]$$

where A is the effective area of the opening, A_o the total cross-sectional area of the pore, r the radius of the pore and a the radius of the molecule. The ratio A/A_o is equivalent to the permeability of the membrane. Data from liposome swelling experiments were plotted on a graph of relative permeability of different PEGs versus the hydrodynamic radius of the PEG. The data were fit using the Renkin equation, and the radius (r) of the best fit curve was taken as the radius of the pore.

Planar BLM Experiments

Planar bilayers were assembled from monolayers by a modification of the technique of Montal and Mueller (1972). Briefly, a 100 μm aperture in a thin Teflon membrane separating two Teflon chambers was primed with hexadecane in *n*-pentane (1:9 v/v). Monolayers of diphytanoyl-phosphatidylcholine (DPhPC, 25 mg/ml in *n*-pentane) were spread on buffer (BLM buffer) containing 1 M KCl, 5 mM $CaCl_2$ and 5 mM HEPES (pH 7.4) in both chambers. Bilayers were formed by slowly lowering and raising the solution level past the aperture. Bilayer formation was followed by monitoring conductance and capacitance. Detergent-solubilized protein was incubated with 10 volumes of β-sitosterol (1 mg/ml) in BLM buffer containing 2% LDAO on ice for 30 min. Protein (6–13 pmol) was added to the *cis* chamber, and insertion of the channel was monitored by holding the membrane at +10 mV. Voltage-clamp recording was performed using a BC-525C bilayer clamp amplifier (Warner Instruments, Hamden, CT). Analogue data from the amplifier were filtered at 1 kHz and digitized with a Digidata 1322 (Axon Instruments/Molecular Devices, Burlingame, CA) at 10 kHz. The pCLAMP 10 (Axon Instruments) software package was used to generate voltage-clamp commands, acquire membrane currents and analyze digitized data.

Selectivity of OsVDAC4 was estimated by measuring the reversal potential of the channel, with the *cis* chamber containing 150 mM KCl 5 mM $CaCl_2$ and 5 mM HEPES (pH 7.4) and the *trans* chamber containing 15 mM KCl, 85 mM sucrose, 184 mM mannitol, 5 mM $CaCl_2$ and 5 mM HEPES (pH 7.4). Reversal potential was measured by running a potential ramp and measuring the potential at which there was no current flowing.

ATP Transport Experiments

Currents through single VDAC channels were recorded in the presence and absence of 50 mM ATP over a range of potentials. KCl concentration was maintained at 1 M throughout the experiment. Noise was estimated as the root mean square deviation from the mean signal.

Estimation of ATP Concentration Assay

After a sufficient number of channel insertions in the membrane, 100 mM ATP was added to the *cis* chamber while taking out an equal volume of buffer simultaneously. To maintain the osmolarity, on the *trans* side 200 mM mannitol was added while taking out an equal volume of buffer. We collected 20 μl of buffer at a particular time interval from the *trans* side for ATP estimation. The ATP concentration was estimated using the ATP determination kit (Invitrogen, Carlsbad, CA).

Results

Sequence Analysis

A cDNA isolated from a library made from indica rice inflorescence was sequenced and the longest predicted open reading frame found to be similar to plant mitochondrial VDACs (Fig. 1a). The closest matches on a BLAST search were VDACs from *P. glaucum* (PgVDAC1) and *L. japonicus* (LjVDAC2.1). Sequence similarities with animal VDACs were also detected but at much lower significance scores. Three rice VDACs, OsVDAC1–3, have previously been reported; and they are also included in the sequence alignment presented in Fig. 1a.

A more extensive sequence alignment was carried out including representative sequences from fungal (yeast), mammalian (human) and plant VDACs of nonmitochondrial origin (Fig. 1a). A phylogenetic tree constructed from this alignment is presented in Fig. 1b. Interestingly, the relationship with porins from the outer membrane of non-green plastids is significantly closer than that with the VDAC protein from chloroplast (*Pisum sativum*).

The deduced amino acid sequence of OsVDAC4 lacks cysteine and tryptophan residues and is predicted to have an isoelectric point of 9.43. Hydropathy analysis of this sequence revealed a pattern not unlike those reported for VDACs from other sources (Fig. 2a). The sequence was submitted to five servers running secondary structure–predicting algorithms. All predicted one N-terminal α-helix and 19 β-strands, though the boundaries differed from algorithm to algorithm. A residue was considered to part of a strand/helix if predicted by three or more algorithms. The consensus prediction presented in Fig. 2b has 19 β-strands and one N-terminal α-helix. The shortest predicted strand of OsVDAC4 is only six residues in length.

Functional Complementation of Yeast VDAC1 Mutants

The VDAC1 gene is deleted in the yeast strain M22.2, which renders it incapable of growth on media containing nonfermentable glycerol as its sole carbon source at the nonpermissive temperature (37°C). Transformation with OsVDAC4 enables it to grow on glycerol medium at 37°C, whereas transformation with the vector alone had no effect (Fig 3a). RT-PCR analysis was performed to confirm expression of OsVDAC4 mRNA in transformed M22.2 (Fig. 3b).

Purification of Bacterially Expressed OsVDAC4

His-tagged OsVDAC4 was overexpressed in *E. coli* bacterial strain BL21 (DE3)-pLysS and was localized primarily in inclusion bodies (data not shown). The protein

Fig. 1 Comparison of the amino acid sequences of OsVDAC4 with reported VDAC sequences. **a** Alignment of OsVDAC4 protein sequence with selected VDAC sequences. PgVDAC and LjVDAC were the closest matches on the BLAST search. Representative mammalian and fungal VDACs are included for comparison. *Filled triangle* conserved residues, *circle* conserved substitution, *plus* semiconserved substitution. **b** Phylogenetic tree constructed based on the amino acid similarity of VDACs from different sources. *Os Oryza sativa, Pg Pennisetum glaucum, Ta Triticum aestivum, Zm Zea mays*. *Numerical values* indicate average phylogenetic distance calculated between the two sequences

A

```
OsVDAC4        ----MAMKGPGLFSDIGKRAKDLLTKDYTY--DQKLTVSTVSSSGVGLTSTAVKKGGL-- 52
PGVDAC         ----MAMKGPGLFSDIGKKAKDLLTRDYTY--DQKLTVSTVSSSGVGLTSTAVKKGGL-- 52
LjVDAC2_1      -----MSKGPGLFSDIGKKPRDLLTKDYSS--DQKLTVSSYSTAGVALTSTAVKKGGL-- 51
TaVDAC1        ------MGGPGLYSGIGKKAKDLLYRDYQT--DHKFTLTTYTANGPAITATSTKKADL-- 50
OSVDAC1        ------MVGPGLYPEIGKKARDLLYRDYQT--DHKFTLTTYTSNGVAITATSTKKADL-- 50
OsVDAC3        -------MAPGLYTDIGKKTRDLLYRDYGT--HHKFTLTTCTPEGVTITAAGTRKNES-- 49
OsVDAC2        MAAAAPPAGPGLYSDIGKKARDLLYRDYHT--DQKFTLTTYAANGAAITVAGTKKNES-- 56
hVDAC1         ------MAVPPTYADLGKSARDVFTKGYGFG-LIKLDLKTKSENGLEFTSSGSANTETTK 53
yVDAC1         -------MSPPVYSDISRNINDLLNKDFYHATPAAFDVQTTTANGIKFSLKAKQPVKDGP 53
                             •  •+ •+•  +••• •+•       • • • •  •  •• +

OsVDAC4        YTLDVSSVYKYKS--TLVDVKVDTESNISTTLTVFDVL-PSTKLVTSVKLPD---YNSGK 106
PGVDAC         YTLDVSSVYKYKN--TVVDIKVDTESNISTTLTVLDAL-PSTKLVTSVKLPD---YNSGK 106
LjVDAC2_1      SVGDVAALYKYKN--TLIDVKLDTASIISTTLTFTDLL-PSTKAIASFKLPD---YNSGK 105
TaVDAC1        TVGEIQSQIKNKN--ITVDVKANSASNVITTITADDLAAPGLKTILSFAVPD---QKSGK 105
OSVDAC1        IFGEIQSQIKNKN--ITVDVKANSDSNVVTTVTVDELT-PGLKSILSFAVPD---QRSGK 104
OsVDAC3        VFGELQTQLKNKK--LTVDVKANSESDLLTTVTVDEFGTPGLKSILSLVVPD---QRSGK 104
OsVDAC2        IFSEIQSQVKNNN--VSVDVKATSDSKLITTFTVHDLGTPGLKGILSIPFPY---QKSAK 111
hVDAC1         VTGSLETKYRWTEYGLTFTEKWNTDNTLGTEITVEDQLARGLKLTFDSSFSPNTGKKNAK 113
yVDAC1         LSTNVEAKLNDKQTGLGLTQGWSNTNNLQTKLEFANLT-PGLKNELITSLTPG-VAKSAV 111
                  +• •  + ++    +     + + • • +   •    + •      ++     +++

OsVDAC4        VEMQYFHENASFATAVGMKPS-PVVEFSGTAGAQGLAFGAEAGFDTATGKFTKYSAAIGV 165
PGVDAC         VELHYFHENASLATVVGTKPS-PVVELSGTVGAQGVTFGAEAGYDTASGKFTKYTAAIGL 165
LjVDAC2_1      LEVQYFHDHATLTAAAALNQS-PIIDVSATFGTPVIAVGAEAGYDTSSGGFTKYTAGISV 164
TaVDAC1        VELQYLHDYAGINASIGLTAN-PVVNLSGAFGTSALAVGADVSLDTATKNFAKYNAALSY 164
OSVDAC1        FELQYSHDYAGVSASIGLTAS-PVVNLSSVFGTKALAVGADVSLDTATGNLTKYNAGLSF 163
OsVDAC3        LELQYLHEYAGINASVGLNSN-PMVNLSGVFGSKELSVGVDVAFDTATSNFTKYNAALSL 163
OsVDAC2        AEVQYLHPHAGLNAIVGLNAN-PLVSFSGVFGTGAFAVGTDVAFDTATGDFTKYNAGLSH 170
hVDAC1         IKTGYKREHINLGCDMDFDIAGPSIRGALVLGYEGWLAGYQMNFETAKSRVTQSNFAVGY 173
yVDAC1         LNTTFTQPFFTARGAFDLCLKSPTFVGDLTMAHEGIVGGAEFGYDISAGSISRYAMALSY 171
                •  • •                • +    + +      • •   • •   +••   +••

OsVDAC4        TKPDYHAAIVLADKGDTVKVSGVYHLDDKQKSSVVAELTRRLSTNENTLTVGGLYKVDPE 225
PGVDAC         TKPDYHAAFILADKGDTIKVSGVYHLDEKQKASAVAELTRRLSTNVNTLTVGGLYKIDPQ 225
LjVDAC2_1      TKPDASASIILGDKGDSIKASYLHHLDQLKKSAAVAEITRKFSTNENTFTVGGSFAIDHL 224
TaVDAC1        TNQDLIASLNLNNKGDSLTASYYHIVEK-SGTAVGAELTHSFSSNENSLTFGTQHTLDPL 223
OSVDAC1        SNDDLIASLNLNNKGDSLTASYYHIVNH-SATAVGAELTHSFSSNENSLTFGTQHTLDPL 222
OsVDAC3        TNSDLIASLHLNNHGDTLIASYYHLVKHHSNTAVGAELSHSFSRNESTLIFGSQHSLDPH 223
OsVDAC2        TTPDLTAALLLNNKGDSLAASYYHKVSK--TSAVGAELAHSFSSNENTLTFGTQHALDEL 228
hVDAC1         KTDEFQLHTNVN-DGTEFGGSIYQKVNK--KLETAVNLAWTAGNSNTRFGIAAKYQIDPD 230
yVDAC1         FAKDYSLGATLN-NEQITTVDFFQNVNAFLQVGAKATMNCKLPNSNVNIEFATRYLPDAS 230
                  •      •  +      +    •+      + + •      +   • ++  +  •

OsVDAC4        TAVKARLNNTGKLAALLQHEVKPKSVLTISGEFDTKALDRP-PKFGLALALRP 277
PGVDAC         TAVKARLNNTGTLAALLQHELKPKSLLTISGEFDTKALDRA-PKFGLALALKP 277
LjVDAC2_1      TQVRARLNNHGKLGALLQHEIIPKSVLTISSEVDTKALDKN-PRFGLAIALKP 276
TaVDAC1        TLVKARINNSGKASALIQHEFMPKSLCTISAEVDTKAIEKS-SKVGIAIALKP 275
OSVDAC1        TVVKARFNNSGKASALLQHEWRPKSVWTISAEVDTKAIDKS-SKVGIAVALKP 274
OsVDAC3        TTVKARFNNYGMASALVQHEWRPKSLITISGEVDTKAIEKS-TKVGLSLVLKH 275
OsVDAC2        TTVKARFNNFGMASALIQHEFRPKSLVTISTEVDTKAIDKS-SKVGLSLVLKP 280
hVDAC1         ACFSAKVNNSSLIGLGYTQTLKPGIKLTLSALLDGKNVNAGGHKLGLGLEFQA 283
yVDAC1         SQVKAKVSDSGIVTLAYKQLLRPGVTLGVGSSFDALKLSEPVHKLGWSLSFDA 283
               • + ••+•• +       •   •     ••  +•   ••    ••• + • •
```

B

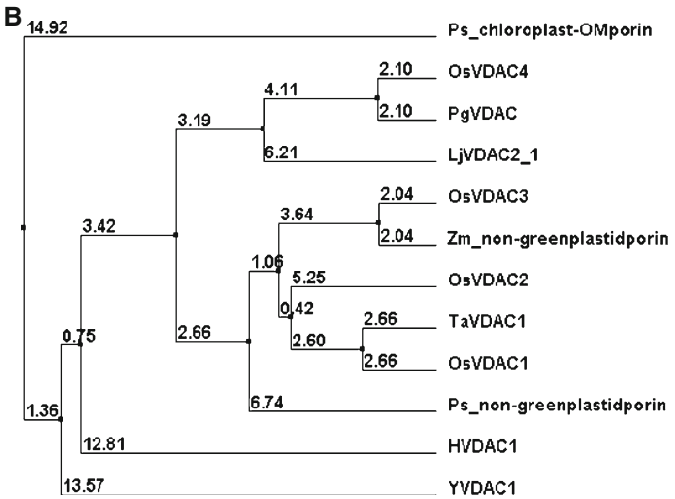

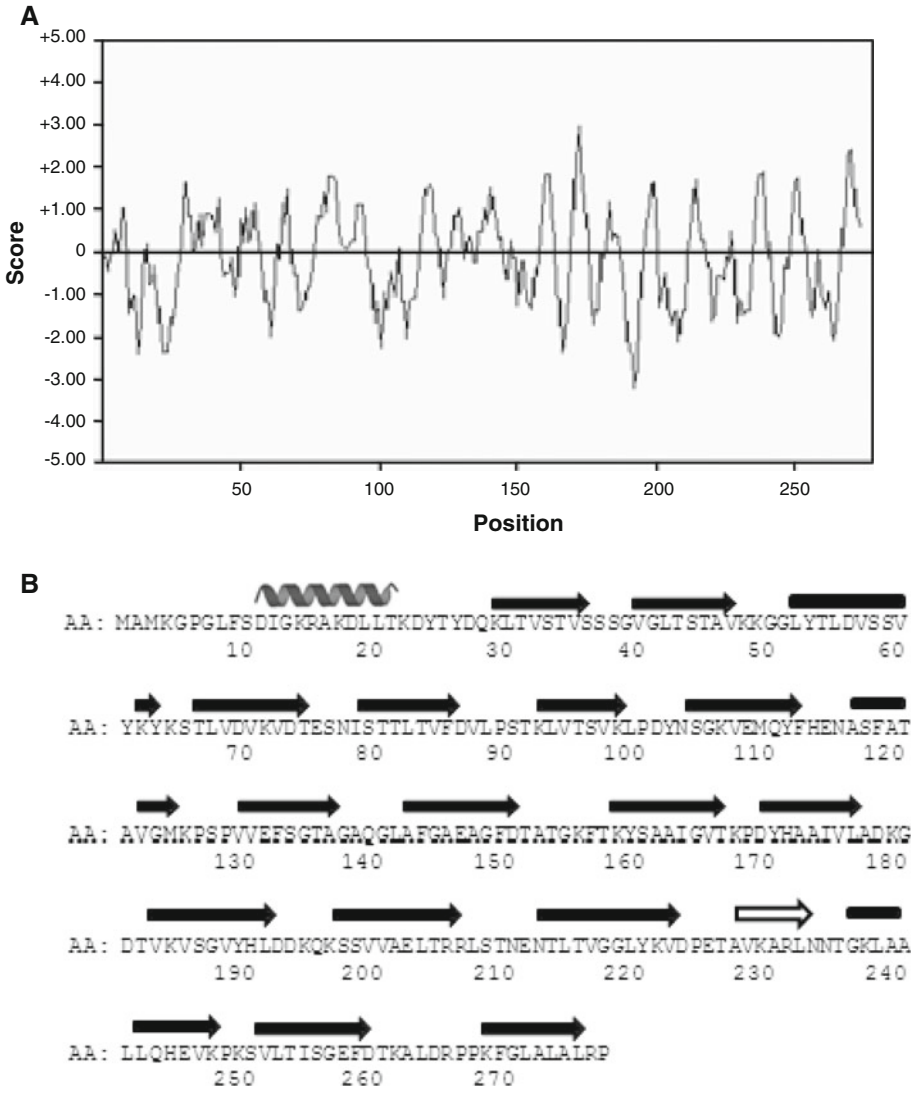

Fig. 2 Hydropathy analysis and secondary structure prediction of OsVDAC4. **a** Hydropathy plot of OsVDAC4 using the Kyte-Doolittle algorithm. **b** Consensus secondary structure prediction of OsVDAC4 based on the output of five different protein structure prediction algorithms (see "Materials and Methods" section). *Spiral* indicates an α-helix and *arrows* indicate *β*-strands. Predicted shortest (six amino acid residue) strand is indicated by *open arrow*

was solubilized from an inclusion body fraction into 6 M guanidine hydrochloride. The solubilized protein bound to Ni-NTA resin on incubation in batch mode and was eluted from the resin after packing into a column. Protein was eluted in buffer containing 50 mM imidazole (lane OsV4 in Fig. 4a). LDAO was added to the eluate to a final concentration of 2% and GnHCl removed by dialysis against loading buffer. The protein obtained was >90% pure as seen on SDS-PAGE (Fig. 4a). Protein stored at –80°C at concentrations of 1–5 mg/ml was stable for 7–8 months.

The major band at 29 kDa was excised from an SDS-polyacrylamide gel, subjected to trypsin digestion and analyzed by MALDI-MS/MS. Several fragments with masses corresponding to those predicted for a tryptic digest of OsVDAC4 were detected. The corresponding peptides are indicated in bold on the sequence in Fig. 4b. Two peptides with masses matching the predicted pattern were sequenced by fragmentation in the spectrometer. The sequences obtained matched those of the predicted tryptic fragments (underlined in Fig. 4b).

Far-UV CD spectra of LDAO-slolubilized protein showed two prominent minima at 208 and 222 nm, indicative of significant α-helical structure and limited *β*-structure. Addition of sterol to the detergent-solubilized protein did not result in a significant change in spectrum (data not shown). However, the CD spectrum of the protein incorporated into liposomes has a broad minimum from 210 to 222 nm. This spectrum is consistent with a mixture of both α-helix and *β*-structure (Fig. 4c).

Estimation of Effective Diameter of the Pore Formed by OsVDAC4 in Liposomes

OsVDAC4 was reconstituted into liposomes by incorporation of detergent-solubilized protein into a multilamellar lipid suspension, which was then repeatedly extruded to

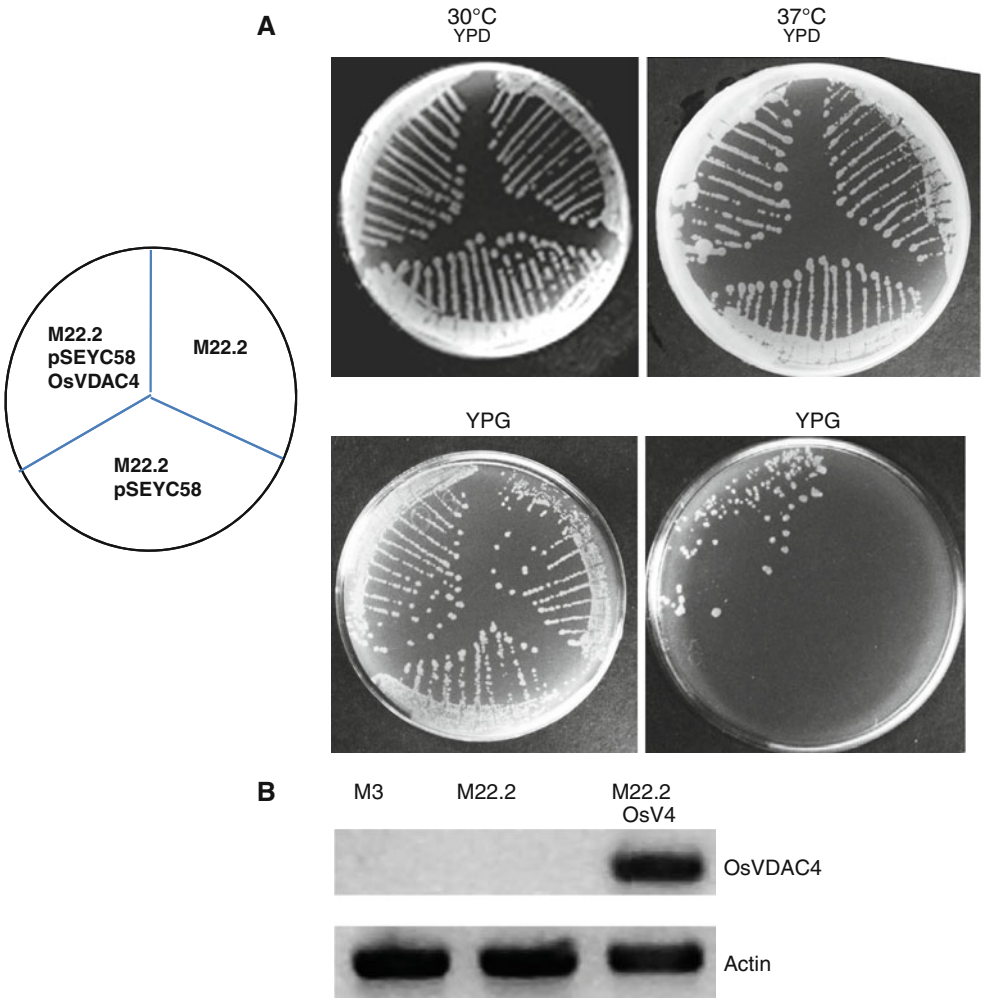

Fig. 3 Yeast complementation analysis. **a** Functional complementation analysis of mitochondrial porin deletion mutant yeast (M22.2) by OsVDAC4. Yeast strain M22.2 was separately transformed with pSEYC58 or pSEYC58-OsVDAC4. The transformants as well as untransformed mutant (M22.2) strains of yeast were streaked on plates containing media supplemented with either dextrose (*first row*) or glycerol (*second row*) as the sole carbon source and incubated separately at 30°C (*first column*) or 37°C (*second column*). Plates were photographed on the fourth day of incubation. **b** RT-PCR analysis of different yeast strains using OsVDAC4 and actin-specific primers

form unilamellar vesicles. Vesiculation was performed in the presence of 10 kDa dextran, which serves as an impermeant solute. Control liposomes formed without protein were diluted into a series of solutions containing varying concentrations of test solute (PEGs), and changes in light scattering associated with swelling or shrinkage of liposomes were monitored as changes in absorbance at 520 nm (Fig. 5a). The solution in which no change in absorbance was observed was deemed to be iso-osmotic with the entrapped dextran solution.

Proteoliposomes prepared in the same batch were diluted into iso-osmotic solutions of a range of PEGs, and the absorbance change was monitored at 520 nm. The initial rate of change in absorbance was taken as an index of the rate of liposome swelling and, hence, of solute transport through the channel. Permeability relative to that of PEG400 was plotted against the hydrodynamic radius of the solute on a semilogarithmic plot (Fig. 5b).

Proteoliposomes swelled rapidly in low–molecular weight PEGs (PEG400 and PEG600), whereas swelling was marginal in high–molecular weight PEG (PEG4000). The data were well fit by the Renkin (1954) equation to estimate the pore diameter. Figure 5b presents data from one set of liposomes, fit by the Renkin equation with $r = 1.29$ nm. Three such experiments yielded an estimate of 1.29 ± 0.02 nm for the radius of the OsVDAC4 pore.

OsVDAC4 Forms High-Conductance Channels in BLM

LDAO-solubilized OsVDAC4 (6–13 pmoles) was added to the *cis* compartment of a BLM chamber after incubation with β-sitosterol. Step increases in current were observed

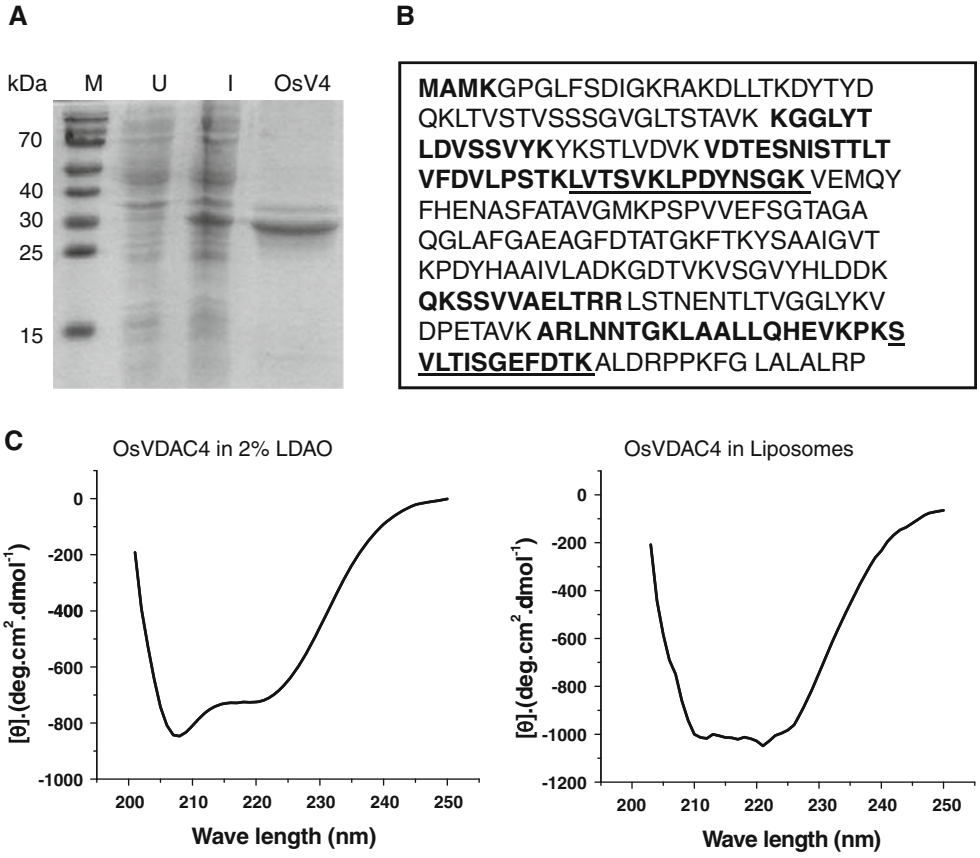

Fig. 4 Purification, sequence analysis and characterization of OsVDAC4. **a** SDS-polyacrylamide gel of whole-cell lysates of uninduced (*U*) and induced (*I*) cultures of BL21pLysS cells transformed with OsVDAC4-pET20B+; OsV4 Ni-NTA purified OsVDAC4 in 2% LDAO, *M* molecular weight marker. **b** Predicted amino acid sequence of OsVDAC4. Residues in *bold* correspond to peptides detected by mass spectrometry of a tryptic digest of OsVDAC4. Peptides which were sequenced are *underlined*. **c** Far UV-circular dichroism spectrum of recombinant OsVDAC4 in 2% LDAO at pH 7.0 and after incorporation in the liposomes

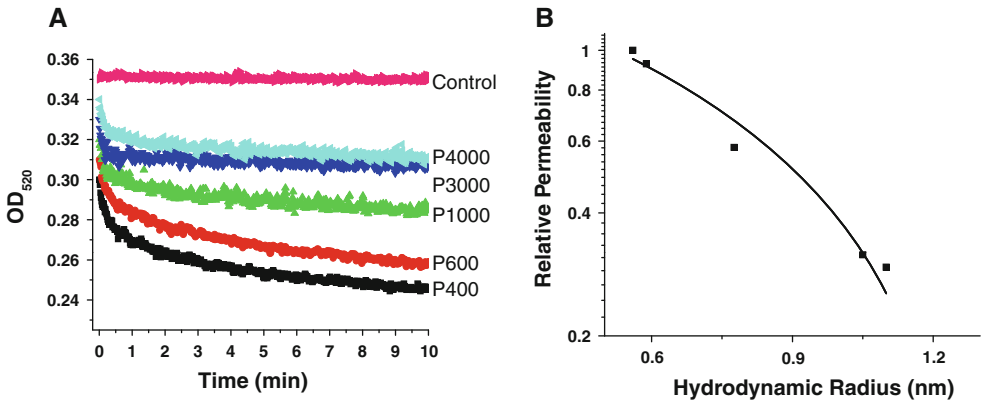

Fig. 5 OsVDAC4 in liposomes. **a** Change in OD_{520} upon dilution of liposomes into buffer containing PEGs at iso-osmotic concentrations. *Control* liposomes diluted into iso-osmotic solution of PEG4000, *P* proteoliposomes diluted into iso-osmotic PEG solutions. Size of the PEG used is indicated against the traces. **b** Permeability of PEGs derived from the data in (**a**), normalized to permeability of P400 and plotted against hydrodynamic radius in a Renkin plot

within 20–30 min, indicative of channel insertion. Channel insertion was critically dependent on prior incubation with β-sitosterol. Other sterols such as cholesterol were not effective at promoting insertion (data not shown). We often observed multiple steps of current increase following the initial insertion (see inset of Fig. 6a for a representative trace with two insertion events). A histogram of the conductance steps observed over 53 insertion events is overlaid with a gaussian in Fig. 6a. The estimated single-channel conductance is 4.53 ± 0.08 nS.

At membrane potentials near zero, channels were present in the highest-conductance, "open" state. On increasing the magnitude of the transmembrane potential, channels transitioned into lower-conductance states. Figure 6b presents a representative triangular voltage ramp applied to a membrane containing three OsVDAC4

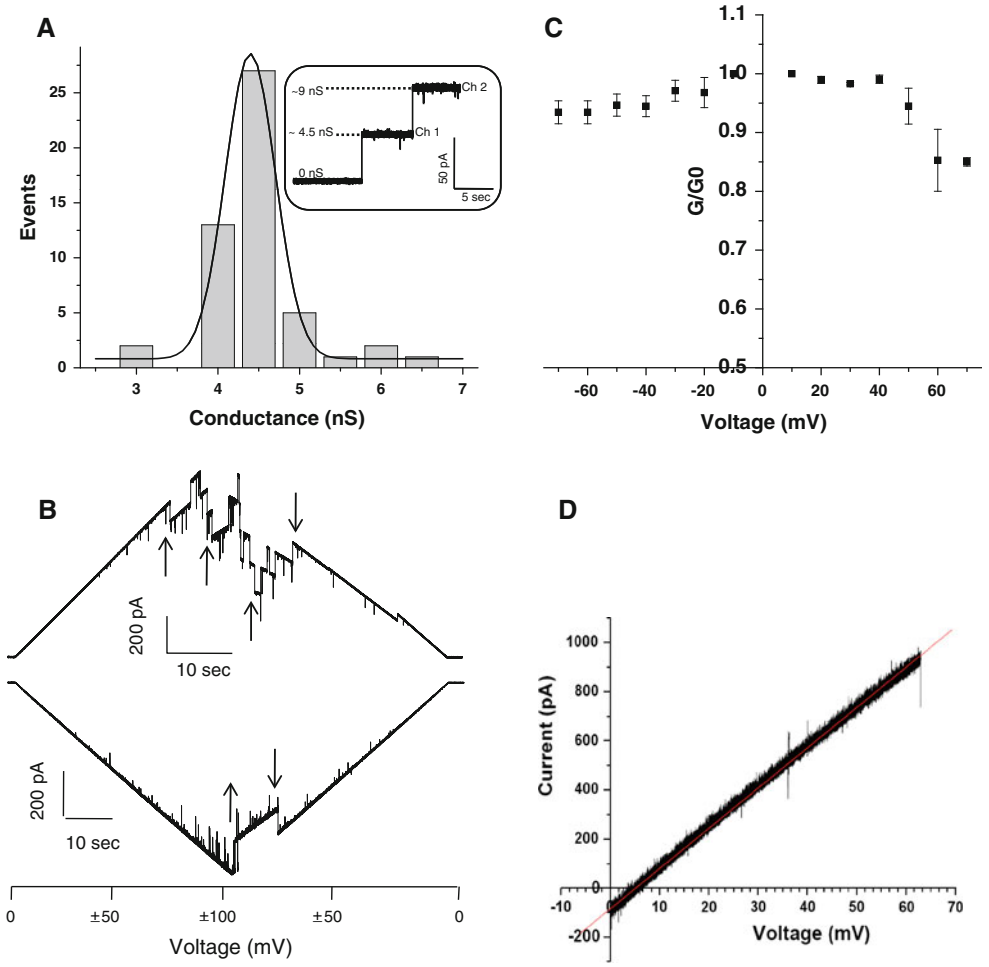

Fig. 6 Electrophysiological characterization of OsVDAC4 in BLM. **a** Histogram of the frequency of insertion events at differing step conductances derived from 53 individual channel insertion events. *Inset* shows insertion of OsVDAC4 into BLM. Current record of a membrane held at +10 mV. Abrupt increase in current indicates channel insertion. This is a representative trace showing two channel insertions. Each channel had ~4.6 nS conductance. **b** Current across a membrane containing three channels, in response to a slow triangular voltage ramp (5 mV/s). *Upper current trace* is representative of positive potential ramp recording; *lower current trace* is representative of negative potential ramp recording. Channels showed transitions to lower-conductance states at large transmembrane potentials (*upward arrows*) and returned to higher-conductance states at lower membrane potentials (*downward arrow*). **c** Voltage dependence of OsVDAC4 conductance. Membrane conductance normalized to that at +10 mV (G/G_{10}) as a function of applied membrane potential (mV) ($n = 5$). **d** Current through a single channel measured in response to a slow voltage ramp (5 mV/s) over the range 0–60 mV. The *cis* compartment contained 150 mM KCl, while the *trans* chamber had 15 mM KCl. The potential at which no current flows is +6 mV. This is a representative trace from one of four such channels

channels. The membrane potential was increased from 0 to +100 mV at 5 mV/s, followed by a decrease from +100 to 0 mV. The membrane was held at 0 mV for at least 3 min before initiating the 0 to –100 to 0 mV negative ramps.

The trace indicates that the channel underwent transitions to subconductance states (indicated by arrows) at large transmembrane potentials. Many more transitions into subconductance states were observed at positive potentials than at negative potentials in this and other ramps (Fig. 6b). Traces acquired at fixed voltage were used to estimate membrane conductance over a range of applied potentials. Figure 6c presents the voltage dependence of conductance normalized to the conductance at 10 mV. The curve is unusually flat at low membrane potential compared to other VDACs, declining only beyond ±60 mV. The decline is sharper at positive potential than at negative potential, consistent with the ramp experiments.

A triangular voltage ramp was applied under asymmetric buffer conditions, with KCl concentrations of 150 mM in the *cis* chamber and 15 mM in the *trans* chamber (Fig. 6d). Data for the rising portion of the ramp are presented over the voltage range 0–60 mV (Fig. 6d). The open channel shows slight anion selectivity as indicated by the measured reversal potential ($n = 3$) of 6 ± 0.6 mV. Selectivity (P_{Cl}/P_K) of OsVDAC4 as

Table 1 Biophysical characteristics of VDACs from different sources

VDACs	Ion selectivity (Cl^-/K^+)	Single-channel conductance (nS)	Channel diameter (nm)	Reference
TaVDAC1 (wheat VDAC1)	1.5	3.8 ± 0.1	–	Elkeles et al. (1997)
TaVDAC2	1.3	4.0 ± 0.1	–	
TaVDAC3	1.6	3.96 ± 0.05	–	
hVDAC1	1.8	4.1 ± 0.1	2–3 nm	Blachly-Dyson et al. (1993)
hVDAC2	1.8	4.0 ± 0.2	–	
Yeast VDAC1	1.8	4.2 ± 0.1	–	
Neurospora crassa VDAC	–	3.4 ± 0.1	2.5 nm	Rostovtseva and Bezrukov (1998)
OsVDAC4	1.33	4.6 ± 0.3	2.6 nm	

calculated using the Goldman, Hodgkin and Katz (GHK) equation is 1.33 (Table 1).

ATP Transport through OsVDAC4 Channels

Electrophysiological studies of VDAC are normally carried out in KCl- or NaCl-containing buffers. Under normal physiological conditions, VDAC is thought to be responsible for transport of biologically important molecules, like ATP, ADP and many organic acids, across the OMM. To check the ability of OsVDAC4 to transport physiologically relevant solutes, we carried out planar bilayer experiments in the presence and absence of ATP. Addition of 50 mM ATP to both chambers of a symmetric membrane resulted in reduction of mean current together with a dramatic increase in root mean square (RMS) noise. Traces at +50 mV for a membrane containing a single channel are presented in Fig. 7a, while Fig. 7b presents mean current and RMS noise of single-channel recordings in the presence and absence of 50 mM ATP over a range of applied potentials. In the absence of OsVDAC4 channels, addition of 50 mM ATP to both chambers did not cause any change in RMS noise (data not shown). It is clear that the increase in noise cannot be explained in terms of increased current

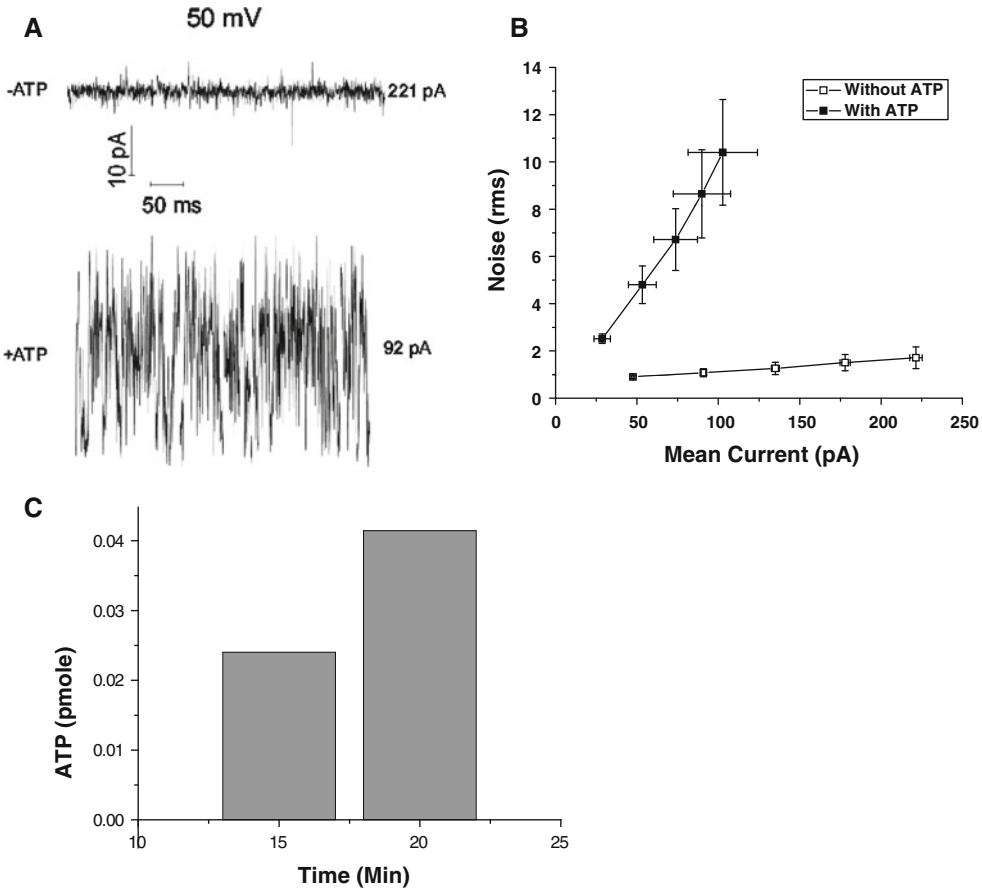

Fig. 7 ATP transport through OsVDAC4. **a** A representative trace at 50 mV showing changes in current noise in the absence and presence of ATP under symmetric buffer conditions. **b** RMS noise and mean conductance through single channels in the presence and absence of 50 mM ATP and potentials ranging from +10 to +50 mV. Each *point* represents mean current and noise (±SE) from four independent channel recordings. *Empty square* channel in the absence of ATP, *Filled square* channel in the presence of 50 mM ATP. **c** Estimation of ATP concentration in the *trans* compartment using luciferin-luciferase assay. ATP 100 mM was added into the *cis* compartment at time 0. One representative experiment out of three

alone but must reflect fluctuations in the rate of charge transport through the channel.

Translocation of ATP was detected by adding 100 mM ATP into the *cis* chamber and maintaining a potential of –10 mV for many minutes. Aliquots taken from the *trans* chamber showed the presence of ATP, the amount increasing with time. Figure 7c shows ATP detected by a luciferin–luciferase assay in an experiment with 30 channels in the membrane. No ATP was detected in the *trans* chamber immediately after addition into the *cis* chamber. Indeed, ATP appeared in the *trans* chamber only after the passage of several minutes, possibly because the *cis* chamber was not stirred.

Discussion

The deduced amino acid sequence of OsVDAC4 shows similarity to plant mitochondrial VDACs, with the closest matches being VDACs from dicotyledonous plants like *P. glaucum* VDAC (PgVDAC) and *L. japonica* VDAC (LjVDAC). A phylogenetic analysis revealed greater evolutionary distance from monocotyledonous mitochondrial VDACs and nongreen plastids. Interestingly, the evolutionary distance to chloroplast VDAC was comparable to those from mammalian and fungal sources.

VDACs from different sources show little conservation of sequence, although all are expected to form β-barrel pores in membranes. Residues in a constituent strand alternate between one that faces the lipid bilayer and another protruding into the aqueous lumen. Thus, they do not exhibit the signature of long hydrophobic stretches characteristic of transmembrane helices. The hydropathy plot for OsVDAC4 (Fig. 2a) is not unlike those reported for other VDACs or bacterial porins.

Three independent structures of mammalian VDAC1 using X-ray crystallography, NMR and a combination of the two techniques reveal 19 β-barrels with an N-terminal α-helix in the pore lumen (Bayrhuber et al. 2008; Hiller et al. 2008; Hiller and Wagner 2009). There are, however, inconsistencies with earlier biochemical and biophysical studies as reviewed in Colombini (2009). A recent determination of yeast VDAC1 topology in mitochondrial membranes also had discrepancies with the published structures (McDonald et al. 2009). It may be noted that all three structures are of protein solubilized by denaturants into detergent micelles from inclusion bodies and consequently not subject to the restrictions of a bilayer environment. The protein we describe in this report is similarly overexpressed in bacteria and solubilized.

OsVDAC4 functionally complements VDAC1 in yeast (Fig. 4a). Not all plant VDACs can successfully complement VDAC deficiencies in other kingdoms. The closely related PgVDAC1, for instance, is targeted to mitochondria when expressed in yeast but does not complement the VDAC1 deficiency (Desai et al. 2006), whereas all wheat VDAC isoforms complement the yeast VDAC deficiency (Elkeles et al. 1997). OsVDAC4 appears to be functional in mammalian cells as well since it participates in death pathways and is subject to regulation by Bcl2 family proteins (Godbole et al. 2003).

We used two different techniques to investigate pores formed by OsVDAC4 in artificial lipid systems. An electrophysiological approach in planar bilayers showed the formation of high-conductance channels that transitioned into lower-conductance states at large transmembrane potentials. These broad characteristics are diagnostic of VDACs from a variety of sources (Table 1). The open-state conductance observed (4.53 ± 0.08 nS) is in the range reported for other VDACs. The voltage dependence revealed by the ramp (Fig. 6b) and the conductance–voltage curve (Fig. 6c) is asymmetric with transitions into lower-conductance states being more frequent at positive membrane potentials than at negative potentials. Most other VDACs display more symmetric voltage dependence (Koppel et al. 1998). The asymmetry in the voltage dependence as well as the voltage range over which the open state is stable have not previously been reported. This may be a consequence of GnHCl solubilization from inclusion bodies into LDAO micelles. However, biophysical properties of *Neurospora crassa* and yeast VDAC purified from mitochondrial membrane as well as bacterial inclusion bodies are shown to be very similar (Koppel et al. 1998). Unfortunately, the behavior of native OsVDAC4 has not been reported so far. Apart from the voltage dependence, the biophysical characteristics of OsVDAC4 are similar to those reported for other VDACs (Table 1).

Addition of ATP led to a decrease in conductance concomitant with an increase in noise. ATP is much larger than Cl^- and is also multiply charged. The lower mobility of ATP should result in lower conductance, while the relatively low frequency of a highly charged ATP ion transiting the pore interspersed with Cl^- would lead to large current fluctuations, as seen in Fig. 7a. The data analyzed are of the channel at potentials between +10 and +50 mV, when the channel is present exclusively in the open state (Fig. 7b). The open state of other VDACs has been shown to conduct ATP and ADP, whereas subconductance states are less permeable to large anions (Rostovtseva and Colombini 1996). Translocation of ATP was confirmed by the detection of ATP in the *trans* chamber over several minutes (Fig. 7c).

The large electrical conductance of the OsVDAC4 channel implies a large-diameter pore through the membrane. We estimated pore size by measuring the rate of permeation of a series of PEGs and consequent swelling of

liposomes. Prior estimates of VDAC diameters have been made using a sieving technique, which yields a lower limit of pore size. The use of liposome swelling to monitor rates of solute transport requires that the experiment be done under iso-osmotic conditions. Osmotic water movement independent of solute flux adds kinetic elements to the liposome swelling phenomenon that complicate its analysis. Under iso-osmotic conditions, liposome swelling is consequent to solute influx, allowing its use as a proxy for transport. The initial rate of swelling is proportional to the rate of solute flux, permitting estimation of the relative rates of permeation of a range of solutes. The data can then be analyzed using the Renkin equation to estimate the diameter of the conducting pore. This approach assumes a cylindrical pore and spherical solutes. Nonetheless, the diameter of OsVDAC4 estimated by the Renkin method yields a pore diameter of 2.58 ± 0.04 nm (Fig. 5), which is closer to that estimated for other VDACs by electron microscopy and crystallography (2.5–2.7 nm) (Dolder et al. 1999; Guo et al. 1995) than that estimated by sieving (3.0 nm) (Colombini 1980, 1987; Sun et al. 1999). These techniques can now be used to study the interaction of VDAC with known modulators of its function.

The bacterially expressed OsVDAC4 protein was localized to inclusion bodies, from which it was solubilized using GnHCl. Removal of denaturant in the presence of detergent resulted in soluble protein–detergent complexes that are largely helical, as seen from the CD spectrum. VDACs from other sources solubilized in detergent have also been reported to have high helical content (Koppel et al. 1998; Shanmugavadivu et al. 2007). This highly helical protein is capable of inserting into either liposomes or planar membranes and forming functional channels. The channels formed have the large conductance and pore diameters characteristic of β-barrel pores. Indeed, CD spectra of protein reconstituted into liposomes suggest that the helical content is reduced while β content is increased. It is conceivable that the sample contains a significant amount of detergent-solubilized protein in addition to liposome-reconstituted protein. Further work, based on the detailed basic characterization of OsVDAC4 presented in this study, on characterizing the structural transition from soluble helical protein to membrane-bound β-barrel, the properties of the resulting pore and mechanisms for modulating the function of VDAC is warranted.

Acknowledgement We thank Prof. Usha Vijayraghavan (Indian Institute of Science, Bangalore, India) for giving us the OsVDAC4 cDNA. The gifts of yeast VDAC mutant strain (M22.2) with yVDAC1-N2 and pSEYC58 plasmids from Prof. Mike Forte and Dr. Elizabeth Blachly-Dyson (Oregon Health and Science University, Portland, OR) are gratefully acknowledged. We thank Mr. Adwait Joshi for help in secondary structure analysis, Ms. Pinky Raychaudhuri for introducing the Montal-Mueller technique in the lab and Ms. Kavana and Mr. Tushar Ranjan for help in electrophysiological experiments. A. G. thanks the Department of Biotechnology for a postdoctoral fellowship. A. K. D. thanks the Indian Council of Medical Research for an SRF fellowship. This work was supported by internal funds from NCBS.

References

Al Bitar F, Roosens N, Smeyers M, Vauterin M, Van Boxtel J, Jacobs M, Homble F (2003) Sequence analysis, transcriptional and posttranscriptional regulation of the rice VDAC family. Biochim Biophys Acta 1625:43–51

Bayrhuber M, Meins T, Habeck M, Becker S, Giller K, Villinger S, Vonrhein C, Griesinger C, Zweckstetter M, Zeth K (2008) Structure of the human voltage-dependent anion channel. Proc Natl Acad Sci USA 105:15370–15375

Blachly-Dyson E, Zambronicz EB, Yu WH, Adams V, McCabe ER, Adelman J, Colombini M, Forte M (1993) Cloning and functional expression in yeast of two human isoforms of the outer mitochondrial membrane channel, the voltage-dependent anion channel. J Biol Chem 268:1835–1841

Cesura AM, Pinard E, Schubenel R, Goetschy V, Friedlein A, Langen H, Polcic P, Forte MA, Bernardi P, Kemp JA (2003) The voltage-dependent anion channel is the target for a new class of inhibitors of the mitochondrial permeability transition pore. J Biol Chem 278:49812–49818

Colombini M (1980) Structure and mode of action of a voltage dependent anion-selective channel (VDAC) located in the outer mitochondrial membrane. Ann NY Acad Sci 341:552–563

Colombini M (1987) Characterization of channels isolated from plant mitochondria. Methods Enzymol 148:465–475

Colombini M (2004) VDAC: the channel at the interface between mitochondria and the cytosol. Mol Cell Biochem 256–257: 107–115

Colombini M (2009) The published 3D structure of the VDAC channel: native or not? Trends Biochem Sci 34:382–389

Cooper B, Clarke JD, Budworth P, Kreps J, Hutchison D, Park S, Guimil S, Dunn M, Luginbühl P, Ellero C, Goff SA, Glazebrook J (2003) A network of rice genes associated with stress response and seed development. Proc Natl Acad Sci 100:4945–4950

Desai MK, Mishra RN, Verma D, Nair S, Sopory SK, Reddy MK (2006) Structural and functional analysis of a salt stress inducible gene encoding voltage dependent anion channel (VDAC) from pearl millet (*Pennisetum glaucum*). Plant Physiol Biochem 44:483–493

Dolder M, Zeth K, Tittmann P, Gross H, Welte W, Wallimann T (1999) Crystallization of the human, mitochondrial voltage-dependent anion-selective channel in the presence of phospholipids. J Struct Biol 127:64–71

Elkeles A, Breiman A, Zizi M (1997) Functional differences among wheat voltage-dependent anion channel (VDAC) isoforms expressed in yeast. Indication for the presence of a novel VDAC-modulating protein? J Biol Chem 272:6252–6260

Geiger TR, Keith CS, Muszynski MG, Newton KJ (1999) Sequences of three maize cDNAs encoding mitochondrial voltage-dependent anion channel (VDAC) proteins. Plant Physiol 121:686

Gincel D, Zaid H, Shoshan-Barmatz V (2001) Calcium binding and translocation by the voltage-dependent anion channel: a possible regulatory mechanism in mitochondrial function. Biochem J 358:147–155

Godbole A, Varghese J, Sarin A, Mathew MK (2003) VDAC is a conserved element of death pathways in plant and animal systems. Biochim Biophys Acta 1642:87–96

Guo XW, Smith PR, Cognon B, D'Arcangelis D, Dolginova E, Mannella CA (1995) Molecular design of the voltage-dependent, anion-selective channel in the mitochondrial outer membrane. J Struct Biol 114:41–59

Heins L, Mentzel H, Schmid A, Benz R, Schmitz UK (1994) Biochemical, molecular, and functional characterization of porin isoforms from potato mitochondria. J Biol Chem 269:26402–26410

Hiller S, Wagner G (2009) The role of solution NMR in the structure determinations of VDAC-1 and other membrane proteins. Curr Opin Struct Biol 19:396–401

Hiller S, Garces RG, Malia TJ, Orekhov VY, Colombini M, Wagner G (2008) Solution structure of the integral human membrane protein VDAC-1 in detergent micelles. Science 321:1206–1210

Keinan N, Tyomkin D, Shoshan-Barmatz V (2010) Oligomerization of the mitochondrial protein voltage-dependent anion channel is coupled to the induction of apoptosis. Mol Cell Biol 30:5698–5709

Koppel DA, Kinnally KW, Masters P, Forte M, Blachly-Dyson E, Mannella CA (1998) Bacterial expression and characterization of the mitochondrial outer membrane channel. Effects of N-terminal modifications. J Biol Chem 273:13794–13800

Kushalappa KM, Mattoo AK, Vijayraghavan U (2000) A spectrum of genes expressed during early stages of rice panicle and flower development. J Genet 79:25–32

Lacomme C, Santa Cruz S (1999) Bax-induced cell death in tobacco is similar to the hypersensitive response. Proc Natl Acad Sci USA 96:7956–7961

Lee SM, Hoang MH, Han HJ, Kim HS, Lee K, Kim KE, Kim DH, Lee SY, Chung WS (2009) Pathogen inducible voltage-dependent anion channel (AtVDAC) isoforms are localized to mitochondria membrane in *Arabidopsis*. Mol Cells 27:321–327

Liu MY, Colombini M (1991) Voltage gating of the mitochondrial outer membrane channel VDAC is regulated by a very conserved protein. Am J Physiol Cell Physiol 260:C371–C374

Madesh M, Hajnoczky G (2001) VDAC-dependent permeabilization of the outer mitochondrial membrane by superoxide induces rapid and massive cytochrome *c* release. J Cell Biol 155:1003–1015

McDonald BM, Wydro MM, Lightowlers RN, Lakey JH (2009) Probing the orientation of yeast VDAC1 in vivo. FEBS Lett 583:739–742

Montal M, Mueller P (1972) Formation of bimolecular membranes from lipid monolayers and a study of their electrical properties. Proc Natl Acad Sci USA 69:3561–3566

Nikaido H, Rosenberg EY (1981) Effect on solute size on diffusion rates through the transmembrane pores of the outer membrane of *Escherichia coli*. J Gen Physiol 77:121–135

Rapizzi E, Pinton P, Szabadkai G, Wieckowski MR, Vandecasteele G, Baird G, Tuft RA, Fogarty KE, Rizzuto R (2002) Recombinant expression of the voltage-dependent anion channel enhances the transfer of Ca^{2+} microdomains to mitochondria. J Cell Biol 159:613–624

Renkin EM (1954) Filtration, diffusion, and molecular sieving through porous cellulose membranes. J Gen Physiol 38:225–243

Rostovtseva TK, Bezrukov SM (1998) ATP transport through a single mitochondrial channel, VDAC, studied by current fluctuation analysis. Biophys J 74:2365–2373

Rostovtseva T, Colombini M (1996) ATP flux is controlled by a voltage-gated channel from the mitochondrial outer membrane. J Biol Chem 271:28006–28008

Salinas T, Duchene AM, Delage L, Nilsson S, Glaser E, Zaepfel M, Marechal-Drouard L (2006) The voltage-dependent anion channel, a major component of the tRNA import machinery in plant mitochondria. Proc Natl Acad Sci USA 103:18362–18367

Shanmugavadivu B, Apell HJ, Meins T, Zeth K, Kleinschmidt JH (2007) Correct folding of the beta-barrel of the human membrane protein VDAC requires a lipid bilayer. J Mol Biol 368:66–78

Shimizu S, Matsuoka Y, Shinohara Y, Yoneda Y, Tsujimoto Y (2001) Essential role of voltage-dependent anion channel in various forms of apoptosis in mammalian cells. J Cell Biol 152:237–250

Shoshan-Barmatz V, Gincel D (2003) The voltage-dependent anion channel: characterization, modulation, and role in mitochondrial function in cell life and death. Cell Biochem Biophys 39:279–292

Shoshan-Barmatz V, Israelson A (2005) The voltage-dependent anion channel in endoplasmic/sarcoplasmic reticulum: characterization, modulation and possible function. J Membr Biol 204:57–66

Shoshan-Barmatz V, Keinan N, Zaid H (2008) Uncovering the role of VDAC in the regulation of cell life and death. J Bioenerg Biomembr 40:183–191

Sun J, Wang YX, Sun MJ (1999) Apoptosis and necrosis induced by sulfur mustard in Hela cells. Zhongguo Yao Li Xue Bao 20:445–448

Tateda C, Yamashita K, Takahashi F, Kusano T, Takahashi Y (2009) Plant voltage-dependent anion channels are involved in host defense against *Pseudomonas cichorii* and in Bax-induced cell death. Plant Cell Rep 28:41–51

Tejuca M, Dalla Serra M, Potrich C, Alvarez C, Menestrina G (2001) Sizing the radius of the pore formed in erythrocytes and lipid vesicles by the toxin sticholysin I from the sea anemone *Stichodactyla helianthus*. J Membr Biol 183:125–135

Vander Heiden MG, Chandel NS, Li XX, Schumacker PT, Colombini M, Thompson CB (2000) Outer mitochondrial membrane permeability can regulate coupled respiration and cell survival. Proc Natl Acad Sci USA 97:4666–4671

Vander Heiden MG, Li XX, Gottleib E, Hill RB, Thompson CB, Colombini M (2001) Bcl-xL promotes the open configuration of the voltage-dependent anion channel and metabolite passage through the outer mitochondrial membrane. J Biol Chem 276:19414–19419

Veenman L, Shandalov Y, Gavish M (2008) VDAC activation by the 18 kDa translocator protein (TSPO), implications for apoptosis. J Bioenerg Biomembr 40:199–205

Wandrey M, Trevaskis B, Brewin N, Udvardi MK (2004) Molecular and cell biology of a family of voltage-dependent anion channel porins in *Lotus japonicus*. Plant Physiol 134:182–193

Young MJ, Bay DC, Hausner G, Court DA (2007) The evolutionary history of mitochondrial porins. BMC Evol Biol 7:31

Zalman LS, Nikaido H, Kagawa Y (1980) Mitochondrial outer membrane contains a protein producing nonspecific diffusion channels. J Biol Chem 255:1771–1774